First publ. in: Atmospheric Environment 27A (1993), pp. 1851-1864

COS AND H_2S FLUXES OVER A WET MEADOW IN RELATION TO PHOTOSYNTHETIC ACTIVITY: AN ANALYSIS OF MEASUREMENTS MADE ON 6 SEPTEMBER 1990

U. BARTELL, U. HOFMANN, R. HOFMANN, B. KREUZBURG, M. O. ANDREAE and J. KESSELMEIER

Max Planck Institute for Chemistry, Biogeochemistry Department, P.O. Box 3060, D-55020 Mainz, Germany

(*First received* 3 *May* 1992 *and in final form* 26 *February* 1993)

Abstract—Micrometeorological measurements of the fluxes of carbonyl sulfide (COS) and hydrogen sulfide (H_2S) were performed over wet meadow vegetation in southern Germany during September 1990. This experiment was conducted in order to verify that vegetation is an important sink for atmospheric COS.

A cryo-sampling technique for continuously collecting these trace gases was applied at four different levels above the ground, combined with eddy correlation measurement of the meteorological fluxes and a micrometeorological profile technique. From these data the trace gas fluxes were determined, based on the assumption that chemical constituents are transported in a similar fashion to meteorological parameters.

The observed diel variation of the COS and H_2S fluxes exhibits peak values of (-360 ± 130) ng S(COS) $m^{-2} s^{-1}$ (deposition) and $(+6.7 \pm 2.4)$ ng S(H_2S) $m^{-2} s^{-1}$ (emission).

Using a modified budget model which includes horizontal advection, it is shown that the observed mean profile of COS is consistent with the assumption of a sink for COS at the canopy level.

The observed strong influence of light intensity fluctuations on the fluxes is explained by variations in the bulk Richardson stability number of the atmospheric boundary layer (ABL), which are the result of equally strong variability of the buoyancy-generated turbulent transport.

The chemical potential gradients of COS and CO_2 in the canopy layer indicate that the COS flux observed in the ABL is related to the COS nonequilibrium distribution across the canopy. COS deposition is interpreted on the basis of COS consumption by the carboxylating plant enzymes. Further, the light-driven H_2O emission supports the linkage between trace gas flux and plant photosynthetic CO_2 assimilation. Finally, the observed H_2S emission may be explained by soil biochemistry.

Keyword index: Carbonyl sulfide, vertical profile, diel variation, micrometeorological technique, budget model analysis.

1. INTRODUCTION

Reduced volatile sulfur compounds are important constituents in the sulfur cycle between hydrosphere, lithosphere, biosphere, and atmosphere (Andreae, 1990; Andreae and Jaeschke, 1992). A review on biogenic sulfur emissions was given by Aneja and Cooper (1989), and the role of higher plants in the emission and deposition is discussed by Rennenberg (1991). One of the major uncertainties in the global sulfur budget is the exchange between the atmosphere and terrestrial vegetation, and the biological processes involved still need to be understood (Rennenberg 1991; Kesselmeier 1991).

Carbonyl sulfide (COS) is the most abundant sulfur compound in the troposphere with concentrations around 500 ± 50 pptv (Torres *et al.*, 1980; Rasmussen *et al.*, 1982). As a consequence of its long lifetime (2–7 yr; Johnson, 1981; Khalil and Rasmussen, 1984), the COS concentration in the atmosphere is remarkably constant both vertically and latitudinally, although a general south to north increase was observed by Bingemer *et al.* (1990). COS is the major contributor to the stratospheric sulfate layer during volcanically quiescent periods (Crutzen, 1976). This stratospheric aerosol affects the Earth's radiation balance and climate and is involved in heterogeneous reactions in the stratospheric ozone cycle. In this context, Turco *et al.* (1980) speculated that increasing anthropogenic emissions of COS may lead to climatic changes within the next century. The main natural sources of COS are photochemical decomposition of dissolved organic sulfur compounds (DOS) in the oceans (Rasmussen *et al.*, 1982; Ferek and Andreae, 1983; Johnson and Harrison, 1986; Andreae, 1992) and microbial decomposition of organic matter in soils (Aneja *et al.*, 1979a; 1979b; Adams *et al.*, 1981a; 1981b; Goldan *et al.*, 1987; Lamb *et al.*, 1987). COS-consuming reactions in the atmosphere, such as stratospheric photolysis (Crutzen, 1976) or the reaction with hydroxyl radicals (Ravishankara *et al.*, 1980) remove only about 50% of the COS produced an-

nually (Khalil and Rasmussen, 1984). Sinks for the unaccounted COS are as yet unidentified. While some authors have observed emission of COS by soil/plant systems (Aneja *et al.*, 1979a; 1979b; Adams *et al.*, 1981b; Steudler and Peterson, 1984; 1985; Carroll *et al.*, 1986) and higher plants (Lamb *et al.*, 1987; Rennenberg *et al.*, 1990; Berresheim and Vulcan, 1992), other studies indicate that COS can be taken up and metabolized by plants (Taylor *et al.*, 1983; Brown and Bell, 1986; Brown *et al.*, 1986; Goldan *et al.*, 1987; 1988; Fall *et al.*, 1988; Gaudry *et al.*, 1991, Mihalopoulos *et al.*, 1989) and soils (Castro and Galloway, (1991). These studies give reason to believe that vegetation is an important sink for COS. Obviously, plants switch between emission and deposition. Protoschill-Krebs and Kesselmeier (1992) recently reported that the carboxylating plant enzymes phosphoenolpyruvate carboxylase and ribulose 1,5-bisphosphate carboxylase, which are supported by carbonic anhydrase ($COS + H_2O \rightarrow CO_2 + H_2S$), are efficient consumers of COS (Kesselmeier, 1992). These authors suggest that the photosynthetic pathway is responsible for COS uptake by higher plants. This COS metabolism mechanism would explain the observed correlation between COS deposition to vegetation and CO_2 assimilation (Hofmann *et al.*, 1992a).

As the magnitude and direction of fluxes in the natural environment depend strongly on the time of day, weather, and the growth state of the plants, further field data are needed. Field measurements can also serve to elucidate the importance of microclimatological conditions which cannot be simulated in laboratory studies. Moreover, field experiments together with laboratory studies render possible parameterization and correlation with basic biological processes (i.e. photosynthesis, transpiration) required for modelling fluxes. We therefore measured COS and H_2S fluxes in conjunction with CO_2 deposition and water vapor fluxes (dominated during daytime by plant transpiration) above wet meadow vegetation in southern Bavaria in September 1990.

2. EXPERIMENTAL TECHNIQUES

2.1. *Site and meteorological instrumentation*

The measurement site is located about 60 km south of Munich, Germany ("Eschenloher Moos", 47°37′ N, 11°11′ E, 628 m a.s.l.). A sufficiently flat, homogeneous fetch with low vegetation (15 cm high grass) in a wind sector from 330° to 70° was selected. Vegetation in the selected fetch is represented by natural grassland typically found in this area (straw grass, deficient in nitrogen), where the agricultural activity is limited to cut the grass once in the summer.

The measurement area was bordered, parallel to the main wind direction, by a highway and a glider runway.

The scaffolding of the short sampling tower results in a disturbance of the windfield. To minimize the influence of this disturbance on the sensors, horizontal booms were mounted extending at least 2 m horizontally away from the tower. The data loggers and the caravan housing the laboratory equipment were placed at a distance of 50 m south of the tower.

The vertical arrangement of the sensors with respect to the grass canopy is shown schematically in Fig. 1. The equipment was comprised of the following

Three different radiation sensors were used covering the following wavelength intervals. The broadband radiation budget in the wavelength interval 0.3–60 μm was measured with a double solarimeter based on thermopiles (Net Radiometer, Lambrecht, Göttingen, Germany), the Photosynthetic Active Radiation (PAR, 0.4–0.7 μm) was determined with a silicon quantum sensor (LI-190SA, Li-Cor, Lincoln, Nebraska, U.S.A.) and the global radiation (0.4–1.2 μm) was measured with a pyranometer (LI-200SA, Li-Cor, Lincoln, Nebraska, U.S.A.). To measure the three components of the wind vector and the air temperature together simultaneously, a 3D-ultrasonic anemometer-thermometer (USAT3, Metek, Hamburg, Germany) operating at sampling rates up to 20 Hz was mounted at 5.5 m above the canopy.

The H_2O concentration was measured instantaneously with an infra-red hygrometer (IR2000, Ophir, Lakewood, Colorado, U.S.A.) operating at a wavelength of 2.7 μm, installed at about 1 m distance from the USAT3. The IR2000 itself has a sensing rate of 40 Hz, but the D/A conversion unit reduces the upper limit of the bandwidth to 1 Hz.

Vertical water vapor flux and latent heat flux were determined by combining the signals of the IR2000 and the USAT3 and registering the turbulent fluctuations of the vertical wind component w and the H_2O concentration together which allows to calculate their covariance.

To take into account the above-mentioned limitations in the frequency response and also the spatial separation between the w and the H_2O sensor, which both lead to a reduced covariance, the covariance values calculated from the signals were corrected by applying the structure function of atmospheric turbulence (Moore, 1986).

To measure the mean vertical profile of standard meteorological quantities Pt_{100}-RTD's were used to measure the air temperature and the wet bulb temperature (psychrometers

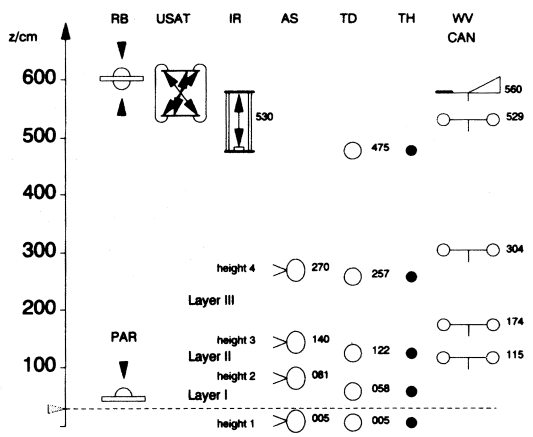

Fig. 1. Sensor configuration used for the micrometeorological measurements. The symbols for the sensors denote the following measured quantities: RB, radiation budget; PAR, photosynthetic active radiation; USAT, instantaneous 3D wind velocity; IR, instantaneous H_2O concentration; AS, averaged trace gas concentration; TD, mean air temperature; TH, mean wet bulb temperature; CAN, mean horizontal wind velocity; WV, mean horizontal wind direction. Between the heights of the sampling inlets, which were mounted at the end of the booms, the air layers are enumerated as indicated in the figure. The arrow at the z-scale denotes the height of the canopy at 15 cm.

manufactured by Thies, Göttingen, Germany), conventional cup anemometers (Lambrecht, Göttingen, Germany) were used to measure the mean horizontal wind velocity at 4 different heights, and the wind direction was registered by a wind vane at one height. All of the sensors were scanned with a rate of 1 Hz and the readings averaged over intervals of 10 min. To establish a correspondence between the meteorological data and the intervals at which the chemical concentration values were taken, 30 min moving averages were calculated afterwards.

2.2. *Air sample analysis*

Reduced sulfur compounds were cryogenically trapped in liquid argon and analysed by gas chromatography (GC)/flame photometric detection (FPD). The air stream was dried by a commercially available Nafion dryer (Model 125, Perma Pure, Toms River, New Jersey, U.S.A.). This drier system was run in a counter current manner with dried ambient air and was shown not to interfere with the sampling of reduced sulfur compounds (Hofmann *et al.*, 1992b). Detection limits for reduced sulfur compounds (2 ℓ air samples) were 10 pptv H_2S, 6 pptv COS, 8 pptv CH_3SH, 3 pptv CS_2, 7 pptv DMS.

Since the FPD detector also responds to CO_2 at the levels present in the atmosphere, it was possible to determine the CO_2 mixing ratio together with those of the reduced sulfur compounds in the air samples.

3. MICROMETEOROLOGICAL METHODS

Various techniques for determining the exchange of atmospheric trace gases with the vegetation layer and measuring the related eddy fluxes in the ABL are described in the literature (see e.g. Fowler and Duyzer, 1989). Among the latest developments, the modified Bowen ratio method (Müller *et al.*, 1993) and the conditional sampling technique (Businger and Oncley, 1990) are reported.

Although it is desirable to apply the eddy correlation technique directly by using fast optical absorption sensors and registering the fluctuations of the trace gas concentration and the vertical wind velocity simultaneously, present analytical limitations restrict this approach in the case of sulfur species to the measurement of the COS flux. The detection limits for this method are, as yet, too high to determine the fluxes of the other reduced sulfur species, e.g. H_2S, DMS and CS_2.

3.1. *Eddy correlation*

In order for the empirical micrometeorological similarity relations of vertical turbulent transport in the ABL to be applied to the determination of the vertical turbulent flux of trace gases in the vicinity of plants, we assume that the physical transport process is the same for different volatile substances in the ABL above the displacement height. This similarity is expressed in the flux profile relation

$$\frac{1}{F^z_{\text{t.g.}}}\frac{\partial \bar{s}_{\text{t.g.}}}{\partial z}=\frac{1}{F^z_{H_2O}}\frac{\partial \bar{q}_{H_2O}}{\partial z} \tag{1}$$

which allows one to determine the unknown vertical trace gas flux $F^z_{\text{t.g.}}$ if the water vapor flux $F^z_{H_2O}$ is determined directly by eddy correlation and the mean vertical gradients of the mixing ratio of trace gas, $\partial \bar{s}_{\text{t.g.}}/\partial z$, and of H_2O, $\partial \bar{q}_{H_2O}/\partial z$, are known from the measurement of the mean vertical profile $\bar{s}_{\text{t.g.}}(z)$ and $\bar{q}_{H_2O}(z)$. Equation (1) is based on the physical fact that the sources of H_2O and trace gas are located at the same height. Above dense vegetation, plant transpiration, which is under strict stomatal control, is the main water vapor source during daylight hours. Trace gases discussed within this work are also exchanged through the stomata, so that the same vertical profile shape resulting from turbulent propagation in the ABL can be expected. However, this applies only to cases where chemical reactions or phase transitions of the trace gas do not take place in the ABL.

The advantage of taking equation (1) as the foundation for our method to determine the flux is that when $F^z_{H_2O}$ is determined directly by eddy correlation no stability correction has to be applied. On the other hand, the same restrictions of horizontal homogeneity and stationarity hold as for the meteorological similarity functions.

3.2. *Flux profile relations*

Since both sides of equation (1) can be expressed in terms of the nondimensional gradient, $\phi^i_{\text{t.g.}}$, the generalized form of equation (1) becomes

$$\phi^i_{\text{t.g.}}=\phi^i_{H_2O}=\phi^i_h \tag{2}$$

where

$$\phi^i_{\text{t.g.}}=\phi^i_{\text{t.g.}}(\ell/L(u^*, \theta^*, q^*), s^*_{\text{t.g.}}) \tag{3}$$

is the generalized flux profile relationship which is assumed to be equal between the gas constituent, t.g., and the water vapor, H_2O, and sensible heat, h. The other symbols used, like $i=u, n, s$, denote the index of stability for the unstable, neutral and stable ABL, d is the vertical displacement by the vegetation of the ABL, $\ell=\zeta-d$ where ζ is the vertical coordinate, and d the displacement height, L the Monin–Obukhov stability parameter, u^* the friction velocity, θ^* the heat flux temperature, q^* the H_2O flux humidity, $s^*_{\text{t.g.}}$ the trace gas flux mixing ratio with respect to dry air.

From equation (2), the trace gas flux $F^z_{\text{t.g.}}$ is related to $s^*_{\text{t.g.}}$ by

$$F^z_{\text{t.g.}}=-\kappa u^* \bar{\rho}_{\text{a.}} s^*_{\text{t.g.}} \tag{4}$$

where $\bar{\rho}_{\text{a.}}$ is the mean dry air density and $\kappa=0.35$ is the von Kármán's constant. As $s^*_{\text{t.g.}}$ is needed to determine the vertical flux $F^z_{\text{t.g}}$ the flux profile relations for $\phi^i_{\text{t.g.}}$ have to be specified. For the unstable and stable ABL stratification, the following special flux profile relations were used in this work:

$$\bar{s}^u_{\text{t.g.}}(\ell)=\bar{s}^0_{\text{t.g.}}+0.74\,\bar{s}^*_{\text{t.g.}}\cdot\left(\ln\left(\frac{\ell}{z_0}\right)-2\ln\left(\frac{1+X}{2}\right)\right),$$

$$X=\left(1-9\left(\frac{\ell}{L}\right)\right)^{1/2} \tag{5}$$

$$\bar{s}^{s}_{t.g.}(\ell) = \bar{s}^{0}_{t.g.} + s^{*}_{t.g.} \cdot \left(0.74 \ln\left(\frac{\ell}{z_0}\right) + 4.7\left(\frac{\ell}{L}\right)\right) \quad (6)$$

where $\bar{s}^{0}_{t.g.}$ is defined by the trace gas concentration in height $\ell_0 = z_0/(1+9z_0/4L)^2$ in the unstable and $\ell_0 \approx z_0 \cdot (1-4.7\,z_0/0.74\,L)$ in the stable case. The aerodynamic parameters u^*, θ^* and q^* were obtained from the least-squares fit of the constant flux profile relations (Paulson, 1970) ϕ^i_m, ϕ^i_h and $\phi^i_{H_2O}$, taken from Businger *et al.* (1970), to the averaged profile data of the wind velocity ($\bar{u}(\ell_1) \ldots \bar{u}(\ell_4)$), of the potential temperature ($\bar{\theta}(\ell_1) \ldots \bar{\theta}(\ell_4)$), and of specific humidity ($\bar{q}(\ell_1) \ldots \bar{q}(\ell_4)$). To calculate the parameters by the least-squares fit of the flux profile relations to the measurement data, the function minimization algorithm by James (1989) was used in this work.

From equations (4)–(7) the flux velocity V_f is

$$V_f = -F^z_{t.g.}/(\bar{\rho}_{a.}\bar{s}_{t.g.}) = -\kappa\, u^* s^*_{t.g.}/\bar{s}_{t.g.}. \quad (7)$$

The advantage of this method lies in the fact that no fast trace gas sensors are needed, because only mean values are required; however, this depends on stationarity and horizontal homogeneity which are seldom met in nature.

3.3. *Micrometeorological budget analysis*

In contrast to flux measurements by the chamber or cuvette technique where the trace gas exchange takes place in a finite volume surrounded by rigid walls, in the outside atmosphere the trace gas concentration also varies due to the exchange of air with other volume elements in the ABL, so that the local budget has to be considered. Starting with the averaged budget equation in terms of the mean mixing ratio $\bar{s}_{t.g.}$

$$\underset{\text{I}}{\frac{\partial \bar{s}_{t.g.}}{\partial t}} + \underset{\text{II}}{U\frac{\partial}{\partial x}\bar{s}_{t.g.}} = \underset{\text{III}}{-\frac{1}{\bar{\rho}_{a.}}\frac{\partial}{\partial z}\bar{F}^z_{t.g.}} + \underset{\text{IV}}{Q_{t.g}/\bar{\rho}_{a.}} \quad (8)$$

where term I describes the storage of trace gas in the air, term II is advection in the presence of a mean longitudinal gradient, term III is the dominant part of flux divergence and term IV represents the external sources and sinks which is the uptake and release of trace gas at the plant boundary. When the trace gas is subject to chemical processes described by the local production/decay in the ABL, equation (8) must be supplemented by an appropriate chemical interchange term, and the flux gradient relation equation (11) becomes modified by an effective eddy diffusivity depending on the different time scales of turbulence and chemical reaction (Brost *et al.*, 1988).

In setting up equation (8), the horizontal longitudinal divergence of turbulent flux is neglected because it is generally small compared to advection, i.e.

$$\frac{1}{\bar{\rho}_{a.}}\frac{\partial}{\partial x}\bar{F}^x_{t.g.} \ll U\frac{\partial}{\partial x}\bar{s}_{t.g.} \quad (9)$$

and the transverse divergence of turbulent flux is neglected in view of the large lateral extension of the fetch.

When the special budget equation (8) is applied to layer II, by integrating over z one obtains

$$\frac{\partial}{\partial t}\int_{z_2}^{z_4} dz'\,\bar{s}_{t.g.}(z') = -\int_{z_2}^{z_4} dz'\,U\frac{\partial}{\partial x}\bar{s}_{t.g.} + \frac{1}{\bar{\rho}_{a.}}\bar{F}^z_{t.g.}(z_2) - \frac{1}{\bar{\rho}_{a.}}\bar{F}^z_{t.g.}(z_4) \quad (10)$$

assuming the absence of sources and sinks within this layer. This assumption is justified in view of the low photochemical reaction rate of COS.

In contrast to the flux profile relation equation (2), (3) this relation is particularly useful for assessing the influence of transport by advection and for evaluating the time variation of the trace gas concentration on the flux variation with height. These variations are always present in real meteorological situations, but are disregarded in the ideal conditions required to apply the flux profile relations. If, further, the turbulent vertical trace gas flux is approximated by the flux gradient relation

$$F^z_{t.g.} = -\bar{\rho}_{a.} K \frac{\partial}{\partial z}\bar{s}_{t.g.} \quad (11)$$

the complete turbulent diffusion equation is obtained from equation (8)

$$\frac{\partial \bar{s}_{t.g.}}{\partial t} + U\frac{\partial}{\partial x}\bar{s}_{t.g.} = \frac{1}{\bar{\rho}_{a.}}\frac{\partial}{\partial z}\bar{\rho}_{a.} K \frac{\partial}{\partial z}\bar{s}_{t.g.} + Q_{t.g.}/\bar{\rho}_{a.}. \quad (12)$$

The solution of equation (12) allows for describing the horizontal inhomogeneity as well as time variations of the concentration field.

4. RESULTS

The meteorological conditions on 6 September 1990 are characterized by the values for radiation, temperature and relative humidity at 58 cm height (Fig. 2). The temperature minimum at night was caused by radiative cooling, and a strong inversion of 3 K m^{-1} was observed near the ground. During the day, sunshine caused considerable warming and labilization of the ABL. The synoptic situation is described by a very shallow anticyclonic wedge with weak, large-scale winds. The mean flow was therefore driven by the mountain valley wind system, which reverses direction twice a day.

4.1. *Diel variation of* CO_2, COS *and* H_2S *concentration*

Figure 3a shows the variation of the observed CO_2 mixing ratio throughout the day. At height 1, CO_2 mixing ratios were significantly higher in the morning and in the evening. In daylight conditions, the CO_2 mixing ratio typically increased monotonously from

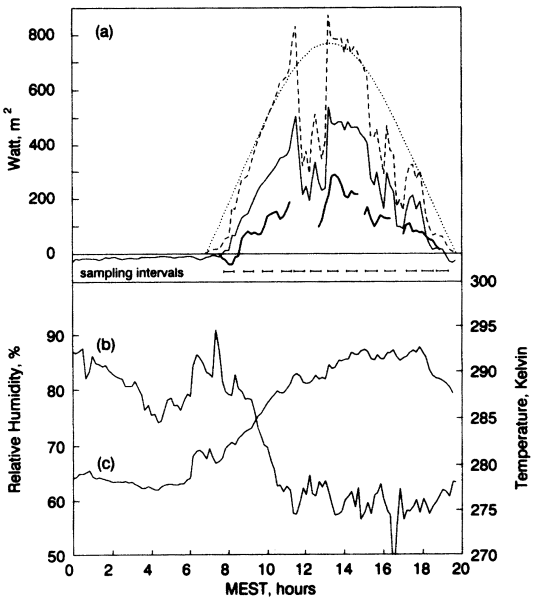

Fig. 2. (a) On 6 September 1990, the diel cycle of the different contributions to the radiation budget (dashed line: short wavelength incoming radiation, continuous line: net radiation) are characterized by fluctuations due to cloudiness. For comparison, the theoretical incoming solar radiation with reference to a horizontally oriented plane is also displayed (dotted line) to indicate the solar culmination point. The latent heat flux (thick line) is derived from the H_2O eddy correlation measurements. (b) Relative humidity at 58 cm, (c) mean air temperature.

the ground to the three sampling heights above the canopy, reflecting plant photosynthetic activity.

For COS mixing ratios (Fig. 3b), values between 750–1100 pptv were found at height 1—with one exception around 17:00 MEST. At that time, a burst of COS was observed at height 1 and the COS increased up to 3500 pptv. At the sample heights above the canopy, COS concentration is 500 pptv in the morning and in the evening, and 3700 pptv in the early afternoon.

H_2S mixing ratios are shown in Fig. 3c: they range between 10 and 65 pptv with maximum values between 9:00 and 14:00 MEST.

4.2. *Diel variation of* COS *flux and* H_2S *flux*

Figure 4a shows the diel variation of the mostly negative (i.e. depositing) COS flux obtained by the eddy correlation method equation (1). Besides the pronounced maximum of the flux at noon in layer II, one notices that the variation of the flux in layer III is less regular, and even reverses its sign sometimes in the early afternoon. The COS flux values in layer III must be regarded with great caution as their error bar is estimated to exceed 100%.

For H_2S, the flux could only be determined in layer II because no significant concentration gradient could be detected in layer III. In Fig. 4b, the diel variation of the predominantly positive (i.e. emissive) H_2S flux is shown. The variation roughly follows that of the COS

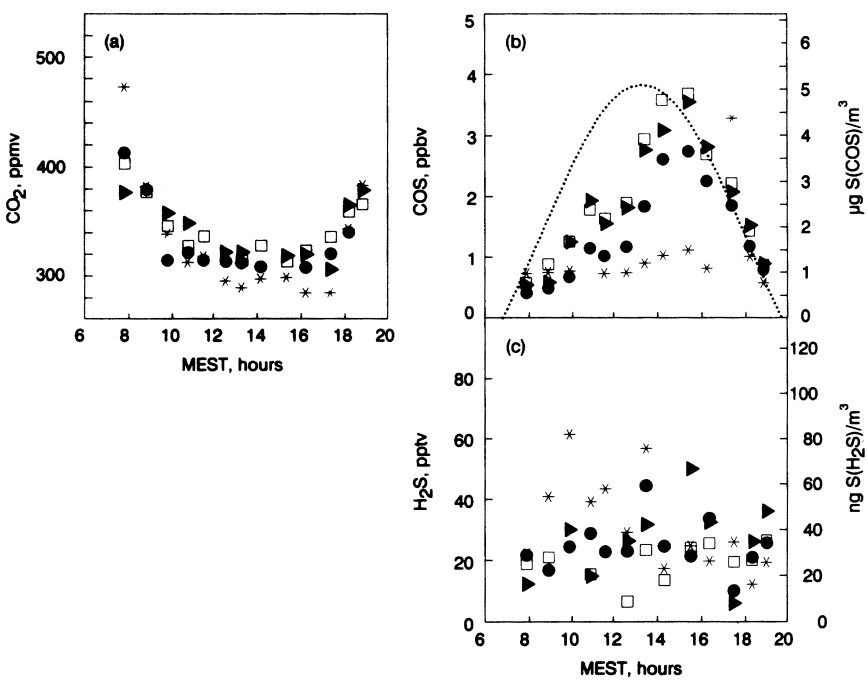

Fig. 3. (a) CO_2 diel cycle at four different levels above ground. The symbols refer to the level heights as follows. *: height 1 (5 cm), ●: height 2 (81 cm), □: height 3 (140 cm), ▲: height 4 (270 cm). (b) COS diel cycle, (c) H_2S diel cycle. The dotted line is the theoretical incoming solar radiation as shown in Fig. 2.

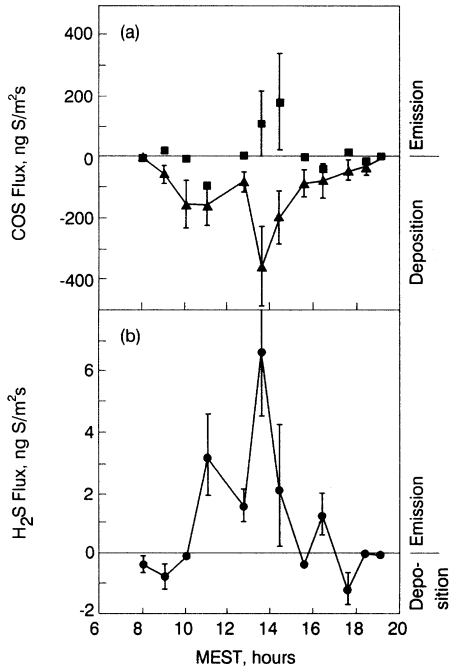

Fig. 4. (a) COS flux derived from the measured H_2O flux and the mean vertical gradients of H_2O and COS using equation (1). ▲: Flux in layer II, ■: layer III. (b) H_2S flux from the vertical gradient of H_2S using the same method as in Fig. 4a. ●: Flux in layer II.

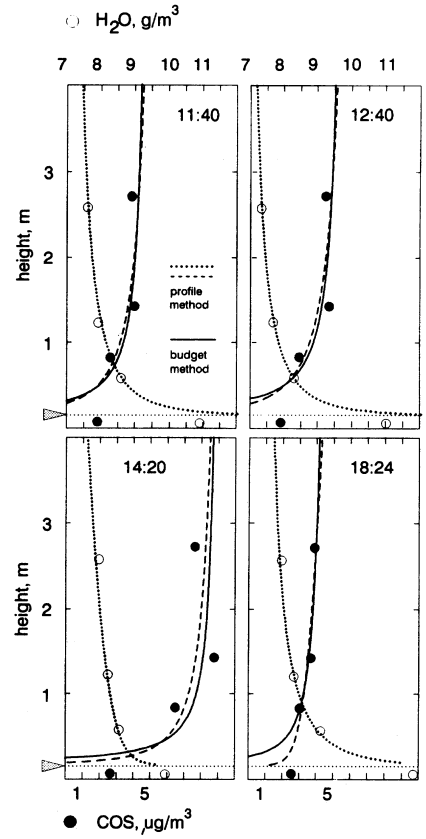

Fig. 5. Vertical COS and H_2O profiles at four representative times (hours indicated are in MEST). The H_2O concentration value at height 475 cm is not displayed in the graph but is always coincident with the fitted profile. To fit equaton (A11) from the *budget model* (continuous line), the constants were put as $d=0.15$ m, $z_0=0.002$ m, $h=0.13$ m, $H=0.08$ m for the displacement height, roughness, mirror height and source height parameters, respectively. For the parameter of the fetch length, x, values of $x=500\text{ m}\pm50\%$ were accepted in the unstable cases. The dotted and dashed lines represent the fitted profiles from the meteorological *profile method* equations (5) and (6). From the vertical profiles of the temperature, humidity and wind velocity, the fluxes of the sensible heat, LS, latent heat, LE and the Monin–Obukhov length L were obtained and have the following values: 11:40, $LS=130\text{ W m}^{-2}$, $LE=310\text{ W m}^{-2}$, $L=-1.6$ m; 12:40, $LS=70\text{ W m}^{-2}$, $LE=260\text{ W m}^{-2}$, $L=-2.9$ m; 14:20, $LS=170\text{ W m}^{-2}$, $LE=400\text{ W m}^{-2}$, $L=-1.6$ m; 18:24, $LS=-21\text{ W m}^{-2}$, $LE=72\text{ W m}^{-2}$, $L=23$ m.

flux with slight deviations in the morning and in the evening.

4.3. COS *mean vertical profiles*

The vertical concentration profiles of COS at four representative times are shown in Fig. 5. The first three profiles at 11:40, 12:40, 14:20 MEST reflect an unstable ABL with very different radiation values, while the fourth profile at 18:24 represents a stably stratified ABL in the early evening. Generally, the COS concentration increases with height indicating a sink of COS near the ground. Note, however, that the COS value at height 3 always exceeds that at height 4, while this anomaly is not observable in the corresponding H_2O profile.

The COS fluxes were derived from the profiles in two ways.

4.3.1. *Flux profile relations.* By fitting the COS flux profile relations ϕ^u_{COS}, ϕ^s_{COS} (equations (5) and (6)) to the data and taking the stability length L from the meteorological profiles, the bias values $\bar{\rho}^0_{\text{COS}}$ and the flux concentration value ρ^*_{COS} were obtained. From this method (referred to as the *profile method*), the COS flux is calculated using equation (4), where u^* was obtained from the fit of the meteorological standard flux profile relation to the measured wind profile.

4.3.2. *Micrometeorological budget analysis.* Since the large difference in the COS vertical flux (Fig. 6a) between two different heights already indicates that the constant flux layer was disturbed, the vertical flux divergence is calculated and compared with the storage contribution obtained by calculating the time derivative of the vertically integrated COS concentration. In spite of the large uncertainty associated with the flux difference estimates, it is evident from Fig. 6a that the storage contribution is 2 orders of magnitude

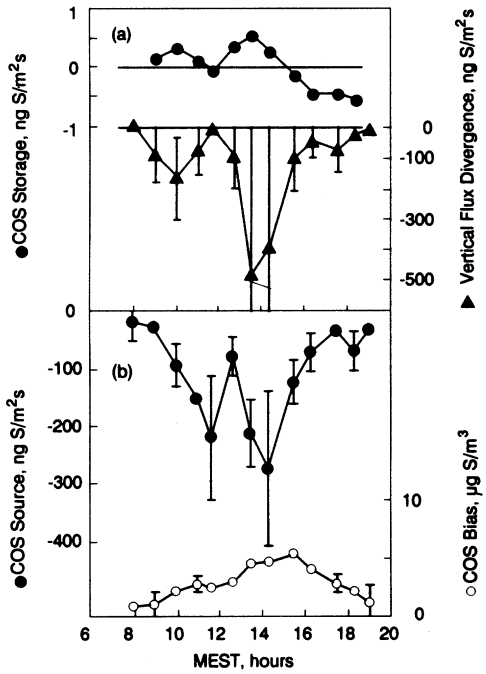

Fig. 6. (a) ●: Storage per unit area contribution to the budget of COS in layer II + layer III (left-hand side of eqution (10)), which was obtained by integrating the density of COS over the vertical thickness of both layers and calculating the time derivative. ▲: Divergence of COS flux across layer II and III from the difference of fluxes between layers II and III (last two terms in equation (10)). For comparison with the COS storage term, note the difference in the scale. (b) Diel cycle of COS source strength (negative values indicate a sink) and corresponding COS bias values as derived from the *budget model* (Section 4.3.2).

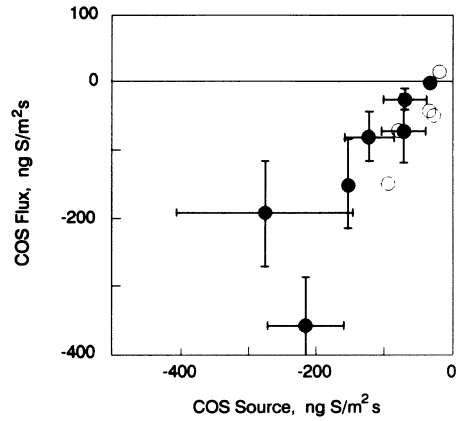

Fig. 7. Comparison of the values for the COS source strength obtained from the *budget model* with the COS flux values by eddy correlation. ●: Mean wind direction coincident with the selected fetch sector, ○: mean wind direction outside of the selected fetch sector.

too small to explain the vertical flux divergence and is neglected in the budget analysis.

Therefore, the second method (referred to as the *budget model*) involves solving the differential equation which results from the budget equation including the advection term, and specifying the source as demonstrated in the appendix (equation (A6)). Fitting the solution equation (A11) to the data, the bias parameter $\bar{\rho}^0_{COS}$ and the source strength parameter Q_{COS} are derived. (To evaluate the vertical dependence of the horizontal velocity $U(\ell)$ and the turbulent exchange coefficient $K(\ell)$ in equation (A11), again the flux profile relations (Businger *et al.*, 1970; Paulson, 1970) were used.)

The diel variation of the COS source strength subsequently obtained is shown in Fig. 6b and correlates well with the COS flux values in the layer II (Fig. 7), with regard to its sign (i.e. uptake) and the variation characteristics. Note that care has to be taken when fitting the profile from the *budget model* (equation (A11)) to the data, as Q_{COS} and x, the effective fetch (c.f. equation (A6)), are strongly correlated parameters. In this work, the size of the fetch was known to be of the order of several hundred meters, so that fits were only accepted with an appropriate value of x, thus reducing the otherwise unavoidable uncertainty in the numerical values for Q_{COS}.

5. RESPONSE OF THE BOUNDARY LAYER TRACE GAS FLUXES TO PLANT ACTIVITY

The main objective of this section is to relate the observed trace gas fluxes in the ABL to the emission and deposition of the various trace gases by the plant canopy.

5.1. *Influence of light on* COS, H_2S *and* H_2O *exchange by plants*

Photosynthesis under light excitation leads through the uptake of CO_2 and the release of H_2O by the plants to a disturbance of the equilibrium distribution of CO_2 and H_2O in the ABL. This disturbance can be described in terms of the gradient of the chemical potential, μ, which in turn gives rise to fluxes directed to or from the plants' surface (Slatyer and Taylor, 1960) in the presence of atmospheric turbulence.

Therefore, it is investigated whether the observed chemical potential gradients and fluxes of the reduced sulfur components, COS and H_2S, can also be traced back to the activity of the plants.

In this work

$$\mu_{t.g.} = \mu^0_{t.g.} + RT \ln(X_{t.g.}) \qquad (13)$$

was used to calculate the chemical potential of the trace gases, where $\mu^0_{t.g.}$ is the standard chemical potential and $X_{t.g.}$ is the mole fraction with respect to humid air. Figure 8b shows the correlation of the COS chemical potential gradient across the canopy (layer I) with photosynthetically active radiation (PAR). Due to the spatial correlation, the gradient in

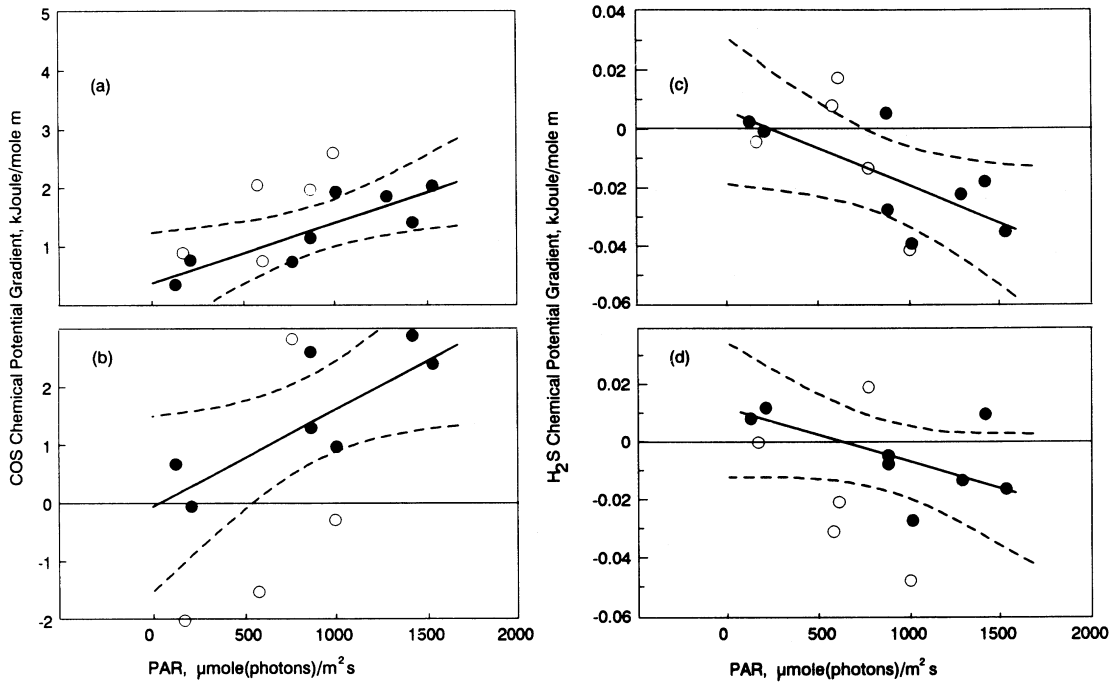

Fig. 8. Plot of the chemical potential gradient of COS ((a), (b)) and H_2S ((c), (d)) vs PAR. (a), (c) across layer II; (b), (d) across layer I. Different symbols are used in the same sense as in Fig. 7. The straight line shows the linear regression of the filled data points together with the hyperbolic "90% confidence region" (dashed lines), calculated with the method by Daniel *et al.* (1980). The regression coefficients are as follows: (a) 1.04 ± 0.2, (b) 1.68 ± 0.4, (c) -0.026 ± 0.008, (d) -0.018 ± 0.008 $(J\ mol^{-1}\ m^{-1})/(\mu mol(photons)\ m^{-2}\ s^{-1})$.

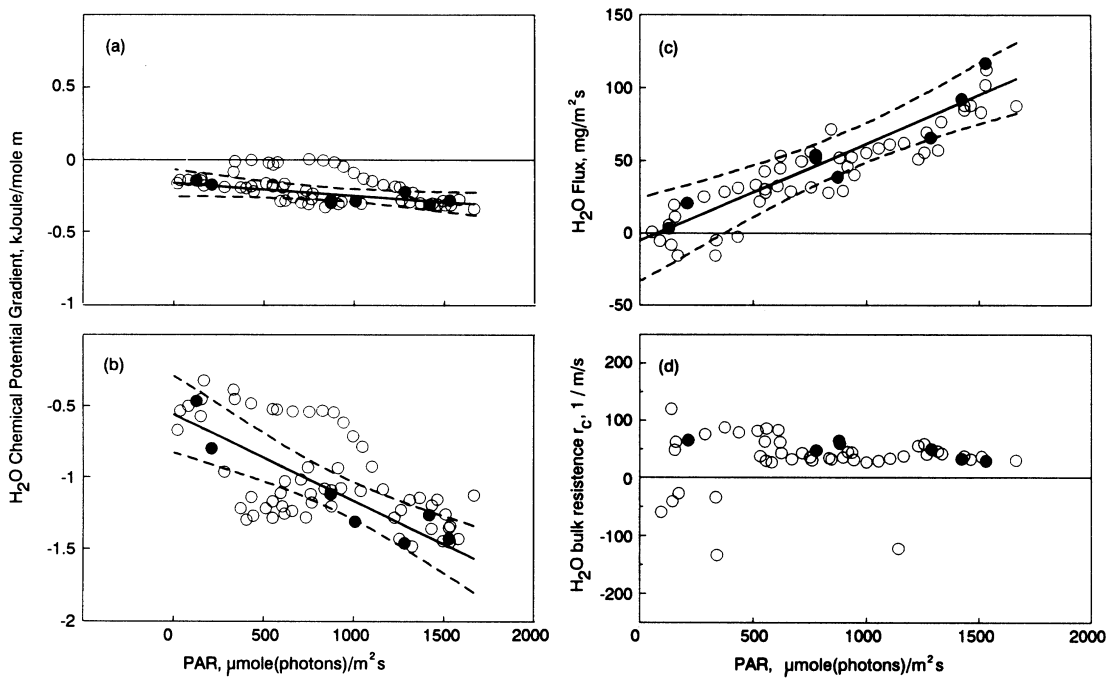

Fig. 9. Plot of the chemical potential gradient of H_2O vs PAR. (a) The gradient 58–122 cm ($\approx$ across layer II), (b) across the canopy (layer I). (c) Relationship between water vapor flux measured by eddy correlation in the level 570 cm above ground and PAR. (d) Relationship between bulk resistance r_c across the canopy layer I for H_2O vapour transport and PAR where $r_c = \Delta\bar{q}_{H_2O}/F^z_{H_2O}$ and $\Delta\bar{q}_{H_2O}$ is the concentration difference of H_2O across layer I. ●: time intervals coincident with the sampling times as in Figs 7 and 8. For the meaning of the lines, see caption of Fig. 8. The linear regression coefficients are as follows: (a) -0.088 ± 0.03, (b) -0.6 ± 0.1 $(J\ mol^{-1}\ m^{-1})/(\mu mol(photons)\ m^{-2}\ s^{-1})$ (c) 67 ± 10 mg H_2O (mmol (photons)).

layer II (Fig. 8a) also correlates with PAR; however, due to mixing resulting from turbulence in the ABL, the gradient is diminished in this layer. Figures 8c and d show the same kind of correlation for H_2S chemical potential gradients. However, the magnitude of the gradient cannot be distinguished between the two layers within the accuracy of the values. Figures 9a and b demonstrate the correlation between H_2O chemical potential gradient and PAR.

The correlation between the COS chemical potential gradient and the chemical potential gradient of CO_2 is shown in Fig. 10, which supports that COS uptake is related to plant activity.

5.2. *Influence of light on trace gas fluxes*

Both the COS flux in layer II (determined by the eddy correlation method, equation (1)) and the COS source strength Q_{COS} (equation (A11), using the mean COS profile alone) exhibit the same correlation with PAR (see Fig. 11).

Before 11:45 MEST, the photosynthetic mechanism of the plants is activated by light, the stratification of the ABL becomes unstable due to warming of the ground and the vertical transport is driven mainly by convection. In this period of time, the ABL is turbulent in all the three observation layers as may be deduced from the Richardson number (see Fig. 12c). Between 11:45 and 13:15 MEST, the study area was obscured by a cloud, evident in Fig. 12a from a 50% reduction in PAR. The COS flux in layer II dropped simultaneously by nearly the same magnitude (Fig. 4), although for the same time period the COS potential gradient in layer I does not exhibit such a sharp drop (Fig. 12b). The increase in the Richardson number (*Ri*) between 304–529 cm indicates a stabilizing of the corresponding layer (Fig. 12c). The same happens in the layer 174–304 cm, whereas in the lowest layer, 115–174 cm, the turbulent state prevails. When the cloud shadow passed, the intermediate layer returned to a weak turbulent state but the upper layer became nearly laminar and remained in this state until evening.

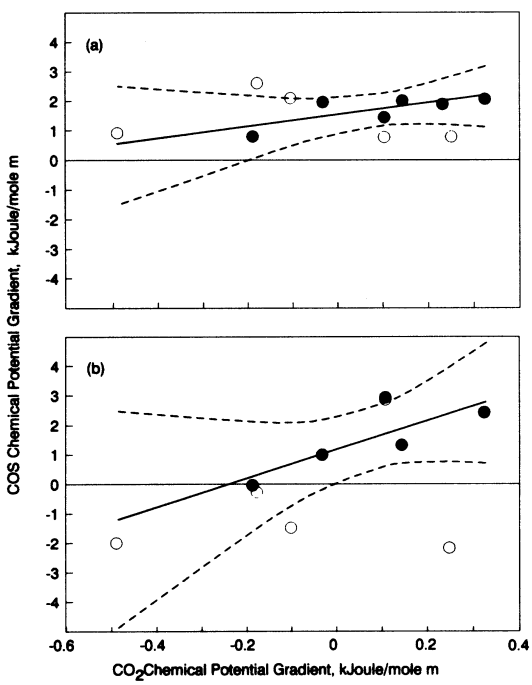

Fig. 10. Plot of the chemical potential gradient of COS vs the chemical potential gradient of CO_2 across layer I. (a) Across layer II, (b) across layer I. For the meaning of the lines, see caption of Fig. 8. The linear regression coefficients are as follows: (a) 2.0 ± 0.9, (b) 4.9 ± 2.

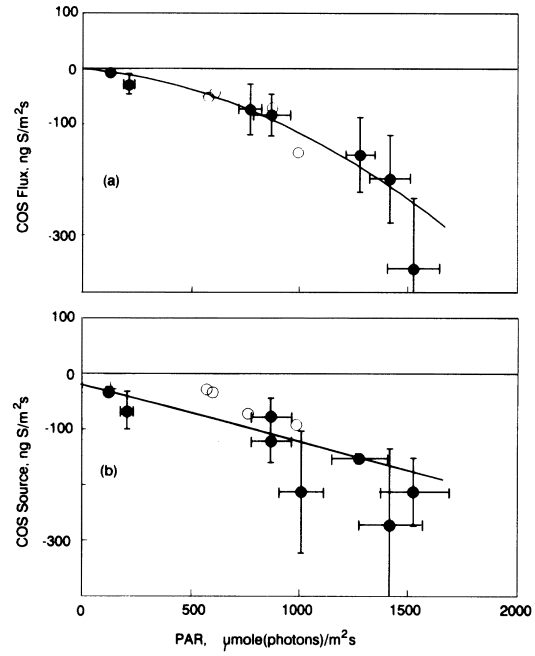

Fig 11. (a) Correlation of the COS flux obtained by eddy correlation with PAR and (b) correlation of COS source strength obtained by fitting equation (A11) to the mean concentration values with PAR. The line is a fit of a 2nd order polynomial to the data (filled symbols). For the COS flux the coefficients are $a_0 = 0.69$ ng S $m^{-2} s^{-1}$, $a_1 = -36 \times 10^{-3}$(ng S $m^{-2} s^{-1}$)/(μmol $m^{-2} s^{-1}$), $a_2 = -80 \times 10^{-6}$(ng S $m^{-2} s^{-1}$)/(μmol $m^{-2} s^{-1}$)^2, and for the COS-source the coefficients are $a_0 = -20$ ng S $m^{-2} s^{-1}$, $a_1 = -102 \times 10^{-3}$(ng S $m^{-2} s^{-1}$)/(μmol $m^{-2} s^{-1}$), $a_2 = -1.03 \times 10^{-6}$(ng S $m^{-2} s^{-1}$)/(μmol $m^{-2} s^{-1}$)^2.

5.3. *Correlation of the trace gas flux and coupling to the ambient chemical potential*

Figure 13 shows the empirical correlation between the vertical COS flux and the H_2O and H_2S flux. Unexpectedly, the COS deposition flux does not depend on the surrounding COS chemical potential monotonously, but exhibits a maximum at about -220 kJ mol^{-1} (Fig. 14). (For the value of the standard chemical potential in the gas phase, $\mu^{gas^0}_{COS} = -169.34$ kJ mol^{-1} was used.) However, since the flux values observed not only differ in chemical

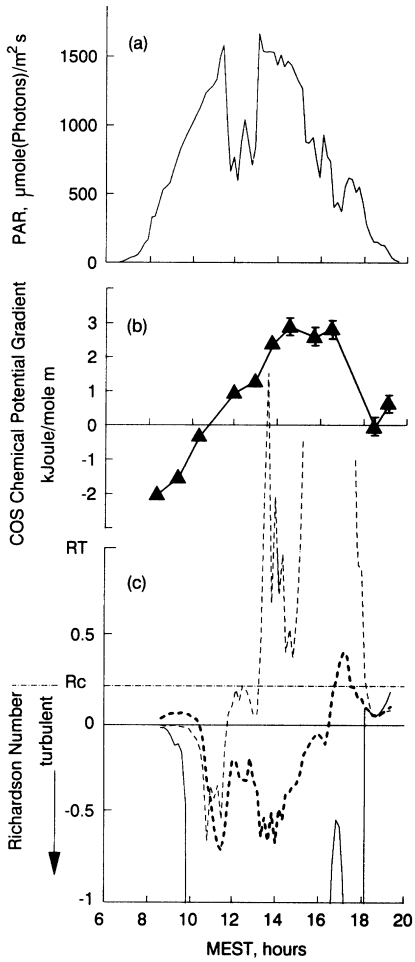

Fig. 12. Response of (a) PAR data, (b) chemical potential gradient of COS across layer I, (c) mean profile derived Richardson number (*Ri*) on the light intensity fluctuation between 11:45 am and 1:15 pm MEST. The continuous line indicates *Ri* in the layer 115–174 cm (~layer I), the thick dashed line in 174–304 cm (~layer II) and the dotted line in 304–529 cm.

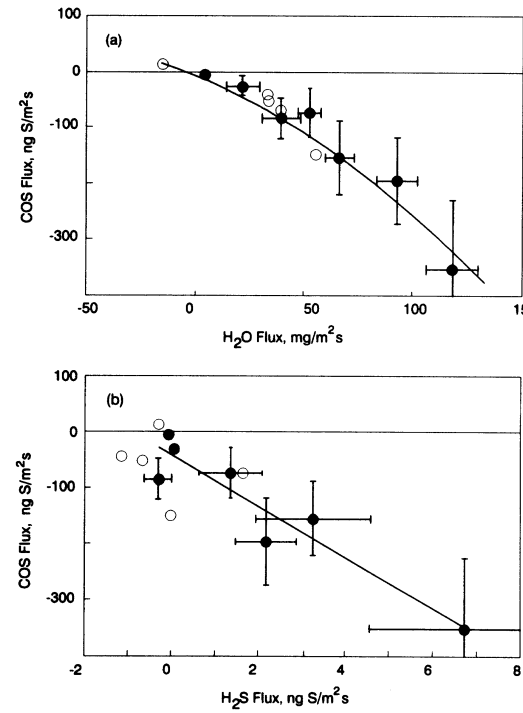

Fig. 13. (a) Correlation between COS flux in layer II and H_2O flux at height 570 cm, (b) COS flux in layer II and H_2S flux in layer II. The line is a fit of a 2nd order polynomial to the data (filled symbols). For the COS flux in (a) the coefficients are $a_0 = -3.2$ ng S m^{-2} s^{-1}, $a_1 = -1600$ ng S m^{-2} s^{-1}/(g$(H_2O)^{-1}$ m^{-2} s^{-1}), $a_2 = -9100$ (ng S m^{-2} s^{-1})/(g$(H_2O)^{-1}$ m^{-2} s^{-1})^2, and for the COS flux in (b) the coefficients are $a_0 = -41$ ng S m^{-2} s^{-1}, $a_1 = -45$ (ng S m^{-2} s^{-1})/(ng(S) (H_2S) m^{-2} s^{-1}).

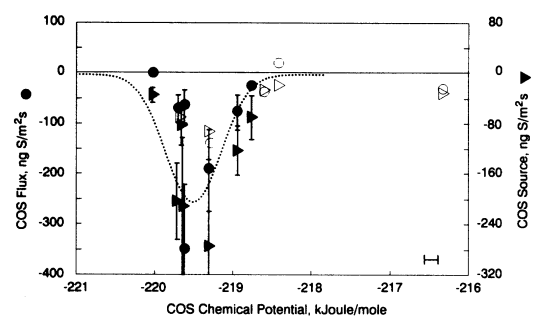

Fig. 14. Dependence of COS flux and COS source strength on the chemical potential of COS at height 1. The dotted line shows the fit of a Gaussian curve to the COS flux points having a width of $500/\sqrt{2}$ J mol^{-1} and a position of -219.5 kJ mol^{-1}. The horizontal bar is the constant error interval for the μ_{COS} values.

potential but also reflect very different light conditions, it is difficult to decide whether an optimum in the environmental COS chemical potential exists. The relationship between this optimum and light intensity remains to be investigated.

6. DISCUSSION AND CONCLUSIONS

The observed variations of CO_2 (Fig. 3a) in the morning and in the evening, when plants cease photosynthetic CO_2 assimilation, and respiration by plants and soil microorganisms is dominating the CO_2-exchange, and its vertical profile clearly reflect plant activity as reported by Biscoe *et al.* (1975) for a crop field.

For COS, a clear diel cycle of the mixing ratios (Fig. 3b) is observed at all three sampling heights which are elevated relative to the tropospheric background. Concentration gradients between heights 3 and 2 point to a deposition of COS, whereas the

concentration differences between heights 4 and 3 are in some cases too low to permit any gradient interpretation. In contrast to CO_2 and COS, no cycle for H_2S (Fig. 3c) was identified from the samples taken above the canopy. Only the mixing ratios at height 1 indicate a diel cycle. Generally, H_2S concentration gradients between heights 2 and 3 suggest an emission of H_2S by the plant/soil system.

From the COS fluxes (Fig. 4a) determined by the *eddy correlation method*, it is clearly evident that there is a marked systematic vertical flux difference (Fig. 6a) throughout the day, especially in layer II. Because of this discrepancy, budget calculations are made in order to include the effects of advection and non-stationarity.

Using the micrometeorological *profile method*, COS flux values are determined by fitting the special flux profile relations to the COS concentration profile (Fig. 5). However, the observed COS concentration profile shows deviations from the monotonous decrease with height. This irregularity may be compared with the strong non-monotonous behavior of the COS profile observed over a wheat field (Hofmann *et al.* 1992a). In this case, the zig-zag shape of the profile can be explained, at least qualitatively, by the presence of a strong sink of COS in the wheat canopy which is located more than 1 m above the ground, whereas in our case, the profile anomaly appears well above the grass canopy and must rather be attributed to the transport mechanism itself.

Since the premise of the application of the *profile method* is ideal ABL conditions of stationarity and horizontal homogeneity which are seldom met in nature, one may conclude that the boundary conditions necessary for the application of the COS flux profile relation are not well fulfilled in our case.

This conclusion is again supported by the analysis using the *budget model*. The quality of the fit of both models to the data (Fig. 5) is less perfect and exhibits systematic deviations from the measured value at height 3. The profile anomaly therefore remains to be explained.

In order to compare the three different methods, Table 1 compiles the results for the same 4 time periods shown in Fig. 5. The COS flux values obtained by eddy correlation method are in good agreement with the COS source strength, whereas the flux values deduced by the meteorological profile method exceed, in the cases of unstable stratification, the measured COS flux value and the COS source strength, obtained by the budget model, but are in agreement with them in the case of stable stratification.

The quantitative agreement between the COS flux from equation (1) at layer II and the COS source strength from equation (A11) is evident for all time periods (Fig. 7), and suggests that a single mechanism is responsible for the PAR dependence of the COS flux and source strength.

The observed decrease in COS concentration towards the ground and the corresponding downward flux of COS indicates that COS is taken up by the plants. However, since the actual site of the trace gas exchange is in the viscous sublayer which adheres to the canopy and is unsuitable for simple meteorological modelling, we cannot determine the fluxes in this sublayer with our method. On the other hand, the determination of the chemical potential gradient across this layer, which, from a thermodynamic point of view, is the driving force of any flux, is readily possible from the measured mean values of the trace gas concentration, humidity and temperature. For COS, the chemical potential gradient in layer I is positive (Figs 8a and b) under the different light conditions represented by the PAR values. In the case of H_2S and H_2O, it is mostly negative (Figs 8c and d, Figs 9a and b). The chemical potential gradients in layer I, which are regarded as the cause for the trace gas exchange between the atmospheric boundary layer and the plant system, are in agreement with the direction of the observed fluxes in layer II, and indicate nonequilibrium, probably due to the release of H_2S and H_2O and the uptake of COS.

Although in general it is difficult to decide whether the COS flux depends on PAR because of the response of the plants to light or because of the change in small-scale convection due to warming, as any PAR fluctuation is accompanied by an appropriate change in the radiation budget, the observations illustrate the influence of boundary layer dynamics on the vertical

Table 1. COS flux in $\mu g\ S\ m^{-2}\ s^{-1}$ by the different methods (c.f. Sections 4.2, 4.3.)

Time (MEST)	*Eddy correlation* (equation (2)) $F^z_{S(COS)}$		V_f ($cm\ s^{-1}$)	u^* ($cm\ s^{-1}$)	*Profile* (equation (4)) $F^z_{S(COS)}$	*Budget* (equation (11)) $Q_{S(COS)}$	V_f ($cm\ s^{-1}$)
11:40	–		–	19	−0.14 ± 12%	−0.21 ± 40%	3.4
12:40	0.014	(a)		19	−0.13 ± 12%	−0.079 ± 40%	2.5
	−0.073 ± 35%	(b)	3.58				
14:20	0.19	(a)		21	−0.14 ± 13%	−0.27 ± 50%	2.3
	−0.20 ± 42%	(b)	4.80				
18:24	−0.0094	(a)		22	−0.025 ± 18%	−0.069 ± 60%	1.6
	−0.029 ± 70%	(b)	1.65				

(a): layer III, (b): layer II.
u^*: friction velocity (c.f. Section 3.3.), V_f: flux velocity in layer II (see equation (7)).

transport (Fig. 12). These imply that vertical transport is markedly impeded in the upper layer in the afternoon. In this case, the change in the vertical fluxes in response to the light intensity drop (Fig. 4a) is mainly caused by the influence of radiation on the buoyancy-generated ABL turbulence. The plant activity does not seem to be much affected by the light intensity drop (Fig. 12b), and contributes little to this effect, which is consistent with the observed PAR flux never decreasing below an assumed light saturation around 200–300 μmol (photons) m^{-2} s^{-1}.

From the meteorological point of view, the decoupling of the vertical exchange between layer II and the ABL above by the local inversion observed in the layer 304–529 cm must have markedly enhanced the observed COS decrease near the ground caused by the COS sink in the vegetation layer. A shallow inversion layer facilitating the observation of a COS deficit has been reported elsewhere (Mihalopoulos *et al.*, 1989).

The negative coefficient found in the relation between COS and H_2O flux and COS and H_2S flux points to opposing directions in the fluxes. This may be interpreted as an uptake of COS and release of H_2O and H_2S occurring at the same site. While the plants' contribution to the H_2O emission is regulated through the stomata which are controlled by environmental factors like temperature, light and humidity, other H_2O sources (like evaporation from the soil and leaf surfaces) also contribute to the total H_2O flux. Since the H_2O bulk resistance across the canopy (layer I) is independent of PAR (Fig. 9d), the flux dependence on PAR is mainly controlled by stomatal conductance.

While, at least on this particular day and site, a proportionality between the H_2S emission and the deposition of COS (Fig. 13b) emerges, our observations point to an emission of H_2S in the range of only 1–2% of the sulfur deposited as COS to the soil/plant system. This implies that either COS is consumed by the higher plants without releasing H_2S, or, more likely, that a combination of processes prevails involving COS/H_2S exchange by microorganisms in the soil (Miller *et al.*, 1989) and uptake of COS by plants. Further physiological studies are required to resolve this problem.

Acknowledgements—We would like to thank H. Bingemer (University of Frankfurt/Main, F.R.G.), H. Kreilein (University of Göttingen, F.R.G.), R. Brost and F. Meixner (Max Planck Institute for Chemistry, Mainz, F.R.G.) for many helpful discussions. The technical support of H. Rettig (Technische Hochschule Darmstadt, F.R.G.) and the use of his wind tunnel are gratefully acknowledged. We thank C. Harris for the help with the preparation of the manuscript.

This research was partially funded by the Bundesministerium für Forschung und Technologie (BIATEX 07EU718).

REFERENCES

Adams D. F., Farwell S. O., Pack M. R. and Robinson E. (1981a) Biogenic sulphur gas emissions from soils in eastern and south eastern United States. *J. Air Pollut. Control Ass.* **31,** 1083–1089.

Adams D. F., Farwell S. O., Robinson E., Pack M. R. and Bamesberger W. L. (1981b) Biogenic sulphur source strength. *Envir. Sci. Technol.* **15,** 1493–1498.

Andreae M. O. (1990) Ocean–atmospheric interactions in the global biogeochemical sulfur cycle. *Mar. Chem.* **30,** 1–29.

Andreae M. O. (1992) Photochemical production of carbonyl sulfide in seawater and its emission to the atmosphere. *Global biogeochem. Cycles* **6,** 175–183.

Andreae M. O. and Jaeschke W. A. (1992) Exchange of sulfur between biosphere and atmosphere over temperate and tropical regions. In *Sulfur Cycling in Terrestrial Systems and Wetlands* (edited by Howart R. W., Stewart J. W. B. and Ivanov M. V.), pp. 27–61. Wiley, Chichester.

Aneja V. P. and Cooper W. J. (1989) Biogenic sulfur emissions. In *Biogenic Sulfur in the Environment* (review) (edited by Saltzman E. S. and Cooper W. J.), pp. 2–13. ACS Symposium Series, Washington.

Aneja V. P., Overton J. H. Jr., Cupitt L. T., Durham J. L. and Wilson W. E. (1979a) Direct measurements of emission rates of some atmospheric biogenic sulphur compounds. *Tellus* **31,** 174–178.

Aneja V. P., Overton J. H. Jr., Cupitt L. T., Durham J. L. and Wilson W. E. (1979b) Carbon disulphide and carbonyl sulphide from biogenic sources and their contributions to the global sulphur cycle. *Nature* **282,** 493–496.

Berkowicz R. and Prahm, L. P. (1979) Generalization of *K* theory for turbulent diffusion, part I: spectral turbulent diffusivity concept. *J. appl. Met.* **18,** 266–282.

Berresheim H. and Vulcan V. D. (1992) Vertical distributions of COS, CS_2, DMS and other sulfur compounds in a loblolly pine forest. *Atmospheric Environment* **26A,** 2031–2036.

Bingemer H. G., Bürgermeister S., Zimmermann R. L. and Georgii H.-W. (1990) Atmospheric OCS: evidence for a contribution of anthropogenic sources? *J. geophys. Res.* **95/12,** 20,617–20,622.

Biscoe P. V., Clark J. A., Gregson K., McGowan, M., Monteith J. L. and Scott R. K. (1975) Barley and its environment, I. Theory and practice. *J. appl. Ecol.* **12,** 227–257.

Brost R. A., Delany A. C. and Huebert B. J. (1988) Numerical modeling of concentrations and fluxes of HNO_3, NH_3, and NH_4NO_3 near the surface. *J. geophys. Res.* **93,** 7137–7152.

Brown K. A. and Bell J. N. B. (1986) Vegetation—the missing sink in the global cycle of carbonyl sulphide (COS). *Atmospheric Environment* **20,** 537–540.

Brown K. A., Kluczewski S. M. and Bell J. N. B. (1986) Metabolism of (35S)-carbonyl sulphide in perennial ryegrass (*Lolium perenne* L.) and radish (*Raphanus sativus* L.). *Envir. exp. Botany* **26/4,** 355–364.

Businger J. A. and Oncley S. P. (1990) Flux measurements with conditional sampling. *J. atmos. Ocean Technol.* **7,** 349–352.

Businger J. A., Wyngaard, J. C., Izumi Y. and Bradley E. F. (1970) Flux-profile relationships in the atmospheric surface layer. *J. atmos. Sci.* **28,** 181–189.

Carroll M. A., Heidt L. E., Cicerone R. J. and Prinn R. G. (1986) OCS, H_2S and CS_2 fluxes from a salt water marsh. *J. atmos. Chem.* **4,** 375–395.

Castro M. S. and Galloway J. N. (1991) A comparison of sulfur-free and ambient air enclosure techniques for measuring the exchange of reduced sulfur gases between soils and the atmosphere. *J. geophys. Res. D.* **96,** 15,427–15,437.

Crutzen P. J. (1976) The possible importance of CSO for the sulphate layer of the stratosphere. *Geophys. Res. Lett.* **3/2,** 73–76.

Daniel C., Wood F. S. (1980) *Fitting Equations to Data.* Wiley, New York.

Fall R., Albritton D. L., Fehsenfeld F. C., Kuster W. C. and

Goldan P. D. (1988) Laboratory studies of some environmental variables controlling sulphur emissions from plants. *J. atmos. Chem.* **6,** 341–362.

Ferek R. J. and Andreae M. O. (1983) The supersaturation of carbonyl sulphide in surface waters of the Pacific Ocean off Peru. *Geophys. Res. Lett.* **10/5,** 393–396.

Fowler D. and Duyzer J. (1989) Micrometeorologial techniques for the measurement of trace gas exchanges. Dahlem Workshop on Exchange of Trace Gases between Terrestrial Ecosystems and the Atmosphere, 1989.

Gaudry, A., Kanakidou M., Mihalopoulos N., Bonsang B., Bonsang, G. Monfray P., Tymen G. and Nguyen B. C. (1991) Atmospheric trace compounds at a European coastal site, application to CO_2, CH_4 and COS flux determinations. *Atmospheric Environment* **26A,** 145–157.

Goldan P. D., Kuster W. C., Albritton D. L. and Fehsenfeld F. C. (1987) The measurement of natural sulphur emissions from soils and vegetation: three sites in the Eastern United States revisited. *J. atmos. Chem.* **5,** 439–467.

Goldan P. D., Fall R., Kuster W. C. and Fehsenfeld F. C. (1988) The uptake of COS by growing vegetation: a major tropospheric sink. *J. geophys. Res.* **93,** 14,186–14,192.

Hofmann U., Hofmann R. and Kesselmeier J. (1992a) Field measurements of reduced sulfur compounds over wheat during a growing season. In *Precipitation Scavenging and Atmosphere–Surface Exchange. Vol. 2—The Semonin Volume: Atmosphere–Surface Exchange Processes* (edited by Schwartz S. E. and Slinn W. G. N.), pp. 967–977. Hemisphere, Washington DC.

Hofmann U., Hofmann R. and Kesselmeier J. (1992b) Cryogenic trapping of reduced sulfur compounds under the influence of a Nafion drier and cotton wedding as an oxidant scavenger. *Atmospheric Environment* **26A,** 2445–2449.

James F. and Roos M. (1989) MINUIT function minimization and error analysis, release 89.12j, CERN computer center library D506.

Johnson J. E. (1981) The lifetime of carbonyl sulphide in the troposphere. *Geophys. Res. Lett.* **8,** 938–940.

Johnson J. E. and Harrison H. (1986) Carbonyl sulphide concentrations in the surface waters and above the Pacific Ocean. *J. geophys. Res.* **91/D7,** 7883–7888.

Kesselmeier J. (1992) Plant physiology and the exchange of trace gases between vegetation and the atmosphere. In *Precipitation Scavenging and Atmosphere–Surface Exchange. Vol. 2—The Semonin Volume: Atmosphere–Surface Exchange Processes* (edited by Schwartz S. E. and Slinn W. G. N), pp. 949–966. Hemisphere, Washington DC.

Kesselmeier J. (1991) Emission of sulfur compounds from vegetation and global-scale extrapolation. In *Trace Gas Emissions from Plants* (edited by Sharkey Th. D., Holland E. A. and Mooney H. A.), pp. 261–265. Academic Press, San Diego, U.S.A.

Khalil M. K. A. and Rasmussen L. E. (1984) Global sources, lifetimes and mass balances of carbonyl sulphide (OCS) and carbon disulphide (CS_2) in the earth's atmosphere. *Atmospheric Environment* **18,** 1805–1813.

Lamb B., Westberg H., Allwine G., Bambesberger L. and Guenther A. (1987) Measurement of biogenic sulphur emissions from soils and vegetation: application of dynamic enclosure methods with Natusch filter and GC/FPD analysis. *J. atmos. Chem.* **5,** 469–491.

Meyers T. P. (1992) On the use of models to identify critical atmosphere–canopy exchange processes. In *Precipitation Scavenging and Atmosphere–Surface Exchange. Vol. 2—The Semonin Volume: Atmosphere–Surface Exchange Processes* (edited by Schwartz S. E. and Slinn W. G. N.), pp. 1035–1051. Hemisphere, Washington DC.

Mihalopoulos N., Bonsang B., Nguyen B. C., Kanakidou M. and Belviso S. (1989) Field observations of carbonyl sulfide deficit near the ground: possible implication of vegetation. *Atmospheric Environment* **23,** 2159–2166.

Miller A. G., Espie G. S. and Canvin D. T. (1989) Use of carbon oxysulphide, a structural analog of CO_2, to study active CO_2 transport in the cyanobacterium *Synechococcus* UTEX 625. *Plant Physiol.* **90,** 1221–1231.

Moore C. J. (1986) Frequency response corrections for eddy correlation systems. *Boundary Layer Met.* **37,** 17–35.

Müller H., Meixner F. X., Kramm G., Dollard G. J., Fowler D. and Possanzini M. (1993) Determination of HNO_3 dry deposition by the modified Bowen ratio method. *Tellus B* (submitted).

Paulson C. A. (1970) The mathematical representation of wind speed and temperature profiles in the unstable atmospheric surface layer. *J. appl. Met.* **9,** 857–861.

Protoschill-Krebs G. and Kesselmeier J. (1992) Enzymatic pathways for the consumption of carbonyl sulphide (COS) by higher plants. *Botanica Acta* **105,** 206–212.

Rasmussen R. A., Khalil M. A. K. and Hoyt S. D. (1992) The oceanic source of carbonyl sulphide (OCS). *Atmospheric Environment* **16,** 1591–1593.

Ravishankara A. R., Kreutter N. M., Shah R. C. and Wine P. H. (1980) Rate of reaction of OH with COS. *Geophys. Res. Lett.* **7,** 861–864.

Rennenberg H. (1991) The significance of higher plants in the emission of sulfur compounds from terrestrial ecosystems. In *Trace Gas Emissions from Plants* (edited by Sharkey Th. D., Holland E. A. and Mooney H. A.), pp. 217–260. Academic Press, San Diego, U.S.A.

Rennenberg H., Huber B., Schröder P., Stahl K., Haunold W., Georgii H. W., Slovik S. and Pfanz H. (1990) Emission of volatile sulphur compounds from spruce trees. *Plant Physiol.* **92,** 560–564.

Slatyer R. O. and Taylor S. A. (1960) Terminology in plant- and soil-water relations. *Nature* **187,** 922–924.

Steudler P. A. and Peterson B. J. (1984) Contribution of gaseous sulphur from salt marshes to the global sulphur cycle. *Nature* **311,** 455–457.

Steudler P. A. and Peterson B. J. (1985) Annual cycle of gaseous sulphur emissions from a New England Spartina alterniflora marsh. *Atmospheric Environment* **19,** 1411–1416.

Sutton W. G. L. (1943) On the equation of diffusion in a turbulent medium. *Proc. R. Soc.* **A182,** 48–75.

Taylor G. E. Jr., Mc Laughlin S. B., Shriner D. S. and Selvidge W. J. (1983) The flux of sulphur-containing gases to vegetation. *Atmospheric Environment* **17,** 789–796.

Torres A. L., Maroulis P. J., Goldberg A. B. and Bandy A. R. (1980) Atmospheric OCS measurements on project GAMETAG. *J. geophys. Res.* **85/C12,** 7357–7360.

Turco R. P., Whitten R. C., Toon O. B., Pollack J. B. and Hamill P. (1980) OCS, stratospheric aerosols and climate. *Nature* **283,** 283–286.

Wippermann F. (1964) Zur quantitativen Erfassung der Absorption am Erdboden eines sich in turbulenter Strömung ausbreitenden Gases. *Beitr. Phys. Atmos.* **37,** 174–182.

APPENDIX: THE BUDGET MODEL EQUATION

The scale analysis of equation (8) for the micrometeorological budget with regard to the experimental values showed that the vertical divergence of the observed COS fluxes dominates the storage of COS in layer II + layer III (Fig. 6a). This justifies neglecting the term I in equation (8) and, according to equation (12), the local budget is described by the turbulent diffusion equation

$$\left(U\frac{\partial}{\partial x}-\frac{1}{\bar{\rho}_{a.}}\frac{\partial}{\partial z}\bar{\rho}_{a.}K\frac{\partial}{\partial z}\right)\bar{s}_{t.g.}=\frac{Q_{t.g.}}{\bar{\rho}_{a.}}. \qquad \text{(A1)}$$

The subject of two-dimensional diffusion with z-dependent U and K has been already treated in the literature for the case of evaporation into the turbulent ABL from a flat

surface (Sutton, 1943). There, the inclusion of the z-dependence of both K and U leads to exact, although mathematically complicated, solutions. Another model, with constant K and U, has been used to calculate the propagation of a plume originating from a point source having a certain elevation above ground, e.g. a chimney (Wippermann, 1964). In this paper, we follow a similar method, assuming that the shape of the propagating trace gas plume is separated from the spatial inhomogeneity of the turbulent field, as in the model of Berkowicz and Prahm (1979).

Then, for K, U and $\bar{\rho}_{a.}$ independent of the trace gas plume's extension, this differential equation can be solved by means of the G function, which is defined by the homogeneous part of (A1)

$$\left(U\frac{\partial}{\partial x}-K\frac{\partial^2}{\partial z^2}\right)G(z-z',\,x-x')=\delta(z-z')\,\delta(x-x') \quad \text{(A2)}$$

where δ denotes the delta function. By taking the Fourier transform of (A2), one obtains

$$g(k_x,k_z)=\frac{i}{4\pi^2}\frac{1}{Uk_x+iKk_z^2},\quad i^2=-1 \quad \text{(A3)}$$

which characterizes in an isotropic turbulence field the diffusion of a plume with wave numbers k_z, k_x.

Now, taking into account the vertical dependence of the turbulent diffusion field in the ABL by assuming K and U to be a function of the vertical distance $\ell=\zeta-d$ above the canopy, but retaining the same spectral characteristics for the trace gas propagation, the G function pair becomes

$$g(k_x,k_z)=\frac{i}{4\pi^2}\frac{1}{U(\ell)k_x+iK(\ell)k_z^2} \quad \text{(A4)}$$

and

$$G(z-z',x-x')=\frac{1}{\sqrt{(4\pi K(\ell)(x-x')\,U(\ell)}}\times\exp\left(-\frac{(z-z')^2}{4K(\ell)/U(\ell)(x-x')}\right),\quad x'<x \quad \text{(A5)}$$

by again applying the Fourier transformation.

To evaluate $\bar{s}_{t.g.}(z)$, both the propagator function G, and the spatial distribution of the source $Q_{t.g.}$, have to be specified. As the plant activity is assumed to be located at $z-d=-H$ and the margin of the fetch defines $x=0$, the z' and x' dependence of the continuous source $Q_{t.g.}$ becomes

$$Q_{t.g.}(z',x')=Q_0\,\delta(z'-d+H)\theta(x')(1-\theta(x'-L)) \quad \text{(A6)}$$

where Q_0[kg m^{-2} s^{-1}] is the surface source density which may be further modelled by including light intensity dependence, and $\theta(x')$ is the unit step function which describes the fetch length extending from $x'=0$ to $x'=L$.

By folding the G function (A5) with $Q_{t.g.}$ (A6) the vertical trace gas profile $\bar{\rho}_{t.g.}(z)$ is obtained by

$$\bar{s}_{t.g.}(z,x)=\frac{1}{\bar{\rho}_{a.}}\int_{-\infty}^{+\infty}dz'\int_{-\infty}^{+\infty}dx'G(x-x',z-z')\,Q_{t.g}(z',x'). \quad \text{(A7)}$$

When the special source term given by equation (A6) and G given by equation (A5) is inserted into equation (A7), the solution to equation (A1) is

$$\bar{s}_{t.g.}(z,x)=\bar{s}^0_{t.g.}+\frac{Q_0}{\bar{\rho}_{a.}}\sqrt{\left(\frac{x}{\pi K(\ell)U(\ell)}\right)}\times\left(\exp\left(-\frac{a(z)}{x}\right)-\sqrt{\left(\pi\frac{a(z)}{x}\right)}\operatorname{erfc}\left(\sqrt{\left(\frac{a(z)}{x}\right)}\right)\right) \quad \text{(A8)}$$

where $a(z)=\dfrac{(z-d+H)^2}{4K(\ell)/U(\ell)}$ and *erfc* is the complementary error function. This solution is verified by direct differentiation. The horizontal advection term

$$U\frac{\partial}{\partial x}\bar{s}_{t.g.}(z,x)=\frac{Q_0}{\bar{\rho}_{a.}}\sqrt{\left(\frac{U(\ell)}{4\pi K(\ell)x}\right)}\exp\left(-\frac{a}{x}\right) \quad \text{(A9)}$$

vanishes at very large x and, according to equation (A1), the vertical flux divergence also vanishes and the vertical profile becomes homogeneous horizontally. The solution (A8) therefore is in accordance with the assumption of constant flux profiles for $K(\ell)$, $U(\ell)$.

Further, recognizing the special boundary condition that the vertial flux vanishes at $z-d=-h$ below the canopy, i.e. $\bar{s}_{t.g.}$ has to fulfill

$$-\bar{\rho}_a K\left.\frac{\partial\bar{s}_{t.g.}}{\partial z}\right|_{z-d=-h}=0 \quad \text{(A10)}$$

and the vertical trace gas profile is approximated by

$$\bar{s}_{t.g.}(z,x)=\bar{s}^0_{t.g.}+\frac{Q_0}{2\cdot\bar{\rho}_a}\sqrt{\left(\frac{x}{\pi K(\ell)U(\ell)}\right)}\times\left(\exp\left(-\frac{a_+(z)}{x}\right)+\exp\left(-\frac{a_-(z)}{x}\right)-\sqrt{\left(\pi\frac{a_+(z)}{x}\right)}\operatorname{erfc}\left(\sqrt{\left(\frac{a_+(z)}{x}\right)}\right)-\sqrt{\left(\pi\frac{a_-(z)}{x}\right)}\operatorname{erfc}\left(\sqrt{\left(\frac{a_-(z)}{x}\right)}\right)\right) \quad \text{(A11)}$$

where $a_\pm(z)=\dfrac{(z-d+h\pm H)^2}{4K(\ell)/U(\ell)}$. In the absence of an inversion layer above, no other boundary conditions are imposed and splitting the source in a real source at $z-d=H-h$ and a mirror source at $z-d=H-h$ equally of half the strength, equation (A10) is fulfilled by superposing both distributions.

To simplify the model, it was assumed that the trace gas constituent propagates by vertical turbulent diffusion alone from the ABL down to the displacement height $z=d$, although below a certain height $z-d=\delta$ other transport processes than those dominant in the ABL may contribute to the vertical mixing process. For $z<d$ the vertical transport definitely involves both cross turbulent mixing and molecular diffusion and must be described by a separate model (for an evaluation of the model influence on assessing deposition velocities see Meyers, 1992).